Aeration Pipe Design for Free Bubbling Hydrodynamic Optimization of Flat Sheet MBRs

Bing Wang[a,b], Yan Zhang[a], Yuan Fang[a], Kaisong Zhang[b*], Robert W. Field[c,d]

[a] *College of Environmental Science and Engineering/Sino-Canada Joint R&D Centre for Water and Environmental Safety, Nankai University, Tianjin 300071, PR China*

[b] *Key Laboratory of Urban Pollutant Conversion, Institute of Urban Environment, Chinese Academy of Sciences, Xiamen 361021, China*

[c] *Faculty of Engineering and Environment, Northumbria University, Newcastle NE1 8ST, UK*

[d] *Department of Engineering Science, University of Oxford, Oxford OX1 3PJ, UK*

* Corresponding author: KS Zhang, kszhang@iue.ac.cn

Abstract

Having previously established that hydrodynamic effect introduced by an open-end aerator for free bubbling is more effective and economic in fouling amelioration in flat sheet MBRs (FSMBR) than conventional closed-end aerator, this work is focused, through two modifications, on its further optimization in a commercial FSMBR. One relates to the aerators themselves, the other to the central aeration air supply pipe. The aerators are tapered, or to be more precise each one is a frustum *i.e.* that portion of cone which remains after the upper part has been cut off by a plane parallel to its base. Based upon a validated Computational Fluid Dynamics (CFD) study (which accurately predicts bubble size and frequency), hydrodynamic features including flow pattern and velocity distribution through aerators, bubble size and shear stress on membranes were predicted for various implementations of the new design. An extensive study found that to achieve a very high degree of uniformity between different aerators for a full-scale FSMBR (160 sheets), the optimal design featured frustum-designed aerators of length 180 mm with the diameter decreasing from 18 to 9 mm at the open end. Each aerator had four top nozzles of diameter 4 mm, and 20 aerators were attached to a pipe of 1760 mm. Based upon this aerator design, the central aeration pipe diameter was optimized, the shear stress was enhanced and corresponding number of effective channel coverage was enhanced by 25 to 75%.

Key Words

Flat sheet MBR; aerator design; CFD; velocity distribution; shear stress; air consumption.

1. Introduction

The flat sheet membrane bioreactor (FSMBR) is one of the major MBR configurations widely used in wastewater treatment because of its high efficiency of separation, good effluent quality and low sludge volume[1]. Membrane fouling has seriously inhibited its extensive application[2-4]. At present, aeration is the normally used method to ameliorate foiling [5, 6]. However, the low efficiency of air utilization and uneven bubble flow from traditional aeration devices has limited the hydrodynamic effect of bubbling on fouling control, particularly at full-scale[7].

In a full-scale commercial FSMBR, the traditional aeration device normally has a fishbone pattern consisting of a central aeration pipe with small aerators on both sides[8], as shown in Fig, 1. The aeration is designed to give one of two regimes. Either the air flowing out through the nozzles of the aerators is free bubbling or slug bubbling[9]. Motivated by the need to enhance surface shear stress through smarter use of hydrodynamics, and thereby achieve enhanced fouling control, our research group has undertaken a number of numerical and experimental works for both aeration regimes [10-14]. However these studies focused on the aeration process from one aerator, assuming all other aerators would have the same bubble behavior. The assumption that there would be little variation between aerators was taken as a given but in order to have a better understanding FSMBRs at industrial scale some additional fundamental work is required and that was the motivation for the current work.

Particularly for full-scale commercial MBR, where the possibility of making directly observations is highly limited, the CFD (Computational Fluid Dynamics) is a very useful tool [15, 16] to explore the hydrodynamics of gas-liquid two-phase flow. There are several

multi-phase simulation methods for gas-liquid interface calculations, such as Euler-Euler, mixture and VOF (Volume of Fluid) methods. The VOF is generally chosen as it is a more suitable method by which to compute the motion of bubbles in a liquid. This is achieved through incorporating an additional volume fraction equation, which is detailed below in section 2.2.2.

For aeration Liu et al.[17] proposed a bent-sheet system to reduce the uneven slug bubble distribution. In this way, the uniformity of bubbles distribution from different nozzles was enhanced. Past works in our group [18-21] have also addressed practical means to improve shear stress whist reduced energy consumption in the FSMBR system. More recently within our group, Wang and coworkers proposed, and studied through CFD and experimental methods, an intermittent bubbling process with large-coalescence bubbles [22-25]. In addition to this work on slug bubbling they have also proposed new aeration designs for free bubbling process [26] and this is also the subject addressed herein.

Unfortunately, limited research concerning some of the challenges concerning the industrial application of FSMBRs has taken place. With the increase application of super large MBR ($\geqslant$100,000 m^3/d), a large number of membrane sheets need to be installed in one module, hence the length of aeration pipe as well as the number of aerators needs to increase. In this situation, the key question concerning the bubbling processes is its homogeneity. When there is a low air velocity from the nozzles of some aerators, the corresponding hydrodynamic effect will be weak and will result in severe fouling of the corresponding membrane surfaces. Therefore specific questions include, (i) how might the air velocity distribution throughout the pipe and all aerators be controlled to ensure decent uniformity, and (ii) how might the air utilization be kept as low as possible.

In our recent prior work on the application of free bubbling process in a FSMBR, a new aerator design was proven to produce uniformly higher intensity shear stresses on the membrane surfaces at lower air usage[26]. This new design of aerator included an open end instead of traditional closed end, as shown in Fig. 1. This design enhanced the air utilization since the side nozzle produces additional large bubbles, whist the traditional one has fewer bubbles of a size to induce higher shear stress. A secondary reason for adding a side nozzle (the top opening apertures are retained) is that an open end allows any sediment inside an aerator to be discharged. This open-end design was for a standard FSMBR module of 80 ~ 100 membrane sheets for which one could assume that the aerators from the one central pipe would give a near uniform air distribution. This design has been applied commercially by Oxiamembrane Co. Ltd (http://www.oxiamem.com). However, for the much larger water treatments incorporating FSMBRs, further numerical and experiments need to be conducted to optimize air distribution across the aeration system. Thus for the current study the basis was a full-scale FSMBR of 160 sheets of membrane.

The main aim of the study was to investigate the potential benefits of an aeration system in which each aerator is an open-ended frustrum with a top row of nozzles. A frustum is a truncated cone in which the upper part has been cut off by a plane parallel to its base. Thus the side aerators are effectively tapered tubes with an open end. The effect upon air distribution and bubble size of varying the diameter of end aperture was investigated. The end aperture diameter was changed in range of 3 to 18 mm. Specifically five frustum open-end aeration pipe designs were compared with the base cases of an open-end configuration and the traditional closed-end design. Overlaying this investigation a combination of three additional critical parameters were investigated through CFD

simulations: (1) aerator length, (2) diameter of top nozzles on the aerator, and (3) The influence of pipe length (for fixed number of membrane sheets this is equivalent to varying the channel gap).

In order to achieve the hydrodynamic benefit of shear stress intensification in all areas whilst not using excess air in some partitioning inside the central air supply pipe was studied so as to have precise control of the air distribution. The modified pipe was studied with varied pipe diameters, to optimize the air velocity distribution among all aerators. Shear stress was also calculated and compared for a full-scale FSMBR with 160 membrane sheets. In addition, the influence of operating parameters on velocity distribution and the consequential induced shear stress was paid great attention, to enhance the hydrodynamic effect in all channels.

2. Methods

2.1 Experimental study

The free bubbling behavior of different aerator designs were investigated by both

experimental and through CFD studies. The design is based on the industrial normal aeration pipe structure, as shown in Fig. 1, there are four small apertures on the top of aerator in both conventional and new designs, but there is an additional opening in the current new configuration, whist there is dead end in the conventional one. The new design in this study has frustum diameter-varying aerators with an open end. The I.D. of the aerator at the point of attachment to the central pipe is 18 mm whilst the I.D. at the aperture of the open end had values as follows: 3, 6, 9, 12, 15 and 18 mm. A schematic diagram of the experimental system is shown in Fig. 2; the tank dimensions were 600×400×1200 mm

(L×T×H). Bubbly flow from seven aerator configurations was generated, and its development could be observed.

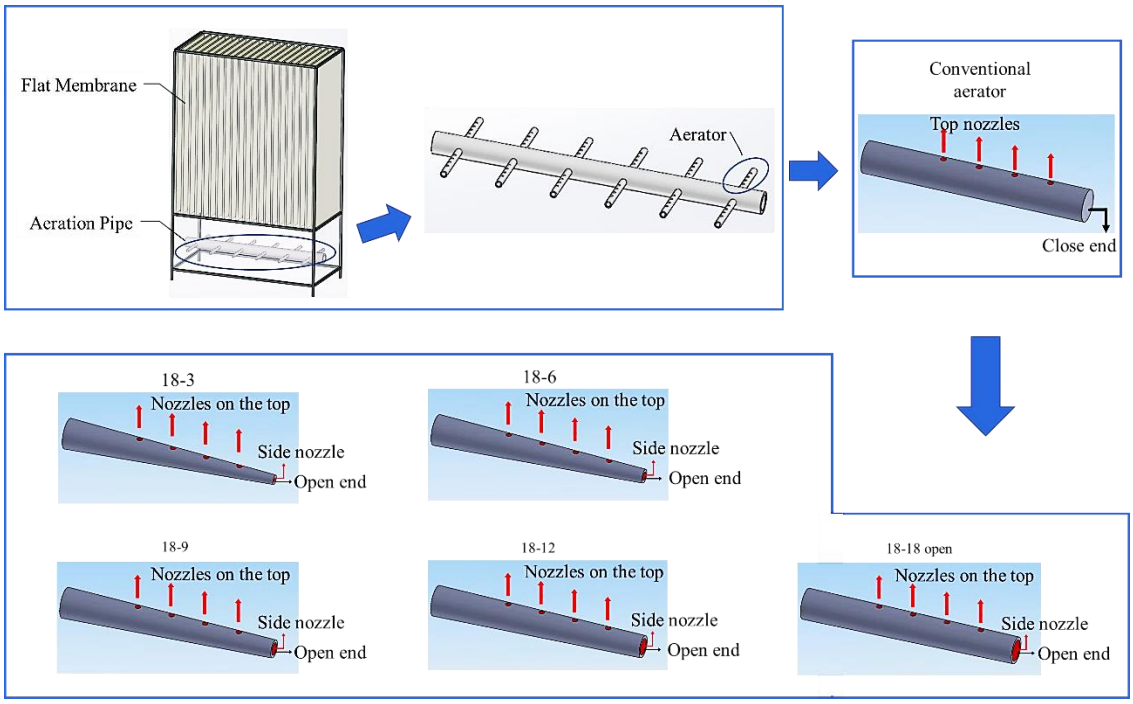

Figure 1 A schematic of the layout for FSMBR with fishbone-type aerator and pictorial summary of the new aerator designs.

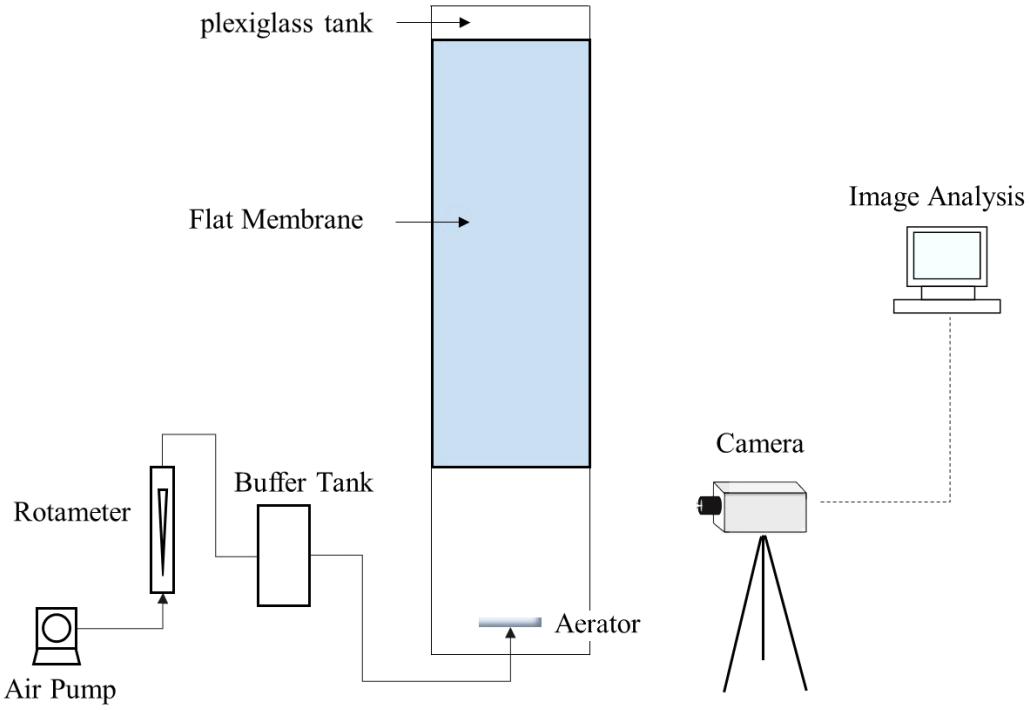

Figure 2 Free bubbling hydrodynamics experimental rig.

The dimensions of membrane sheets were 510×6×1200 mm (L×T×H), and were supplied by Oxiamembrane Co., Ltd, China. Aerators with different designs were fixed 350 mm below the stack of 32 membrane plates. The air supplied via the air flow rotameter was maintained at a flow rate of 96 L/min, which corresponds to the supply in industry for the chosen number of membrane plates.

Bubble behavior was observed and recorded by a video camera to the front. A CMOS camera (FASTCAM SA1.1, Photron, Japan) with 1024×1024-pixel and up to 480 fps high speed was used. It was equipped with a Nikon Micro 60 mm F2.8D lens. Image J was run to process the images and obtain quantitative information on bubble characteristics. The number of bubbles from each nozzle was divided by the time interval of 1 min to obtain the bubble frequency. Experiments were conducted three times at room temperature.

2.2 CFD simulation

2.2.1 Physical model and meshing

To simulate gas-liquid two-phase flow behavior in a FSMBR, 3D computational geometry was built and meshed in GAMBIT 2.4.6. High-quality mesh of Cooper-type hex was used to divide the computing domain. The total number of membrane plates was 160 (Oxiamembrane Co., Ltd, China) and 16 covered by one aerator, so there were 10 pairs of aerators on the central pipe. Owing to the symmetric boundary condition, one only needs to simulate 10 aerators on one side; this saves computational time. Output such as liquid velocity distribution was observed for the various types of aerators for a range of set-ups in which the variables varied were pipe length, aerator length and top nozzle diameter. The ranges were 1520 ~ 2240 mm, 130 ~ 230 mm, and 3 ~ 6 mm, for pipe length, aerator length and top nozzle diameter respectively. A change in pipe length accords with, and is a consequence of, a change in the channel gap. These varied from 3 ~ 8 mm, which is the normal range applied in industry.

After the optimal design of the aerators was determined, modifications to the central air supply pipe were investigated. In general, a series of computational geometries with different pipe designs were set up. A typical mesh is shown in Fig. 3; the highest average EquiSize Skew parameter was 0.658 for the entire computation domain, which indicated high mesh quality. Table 1 shows detailed mesh information for different computational geometries.

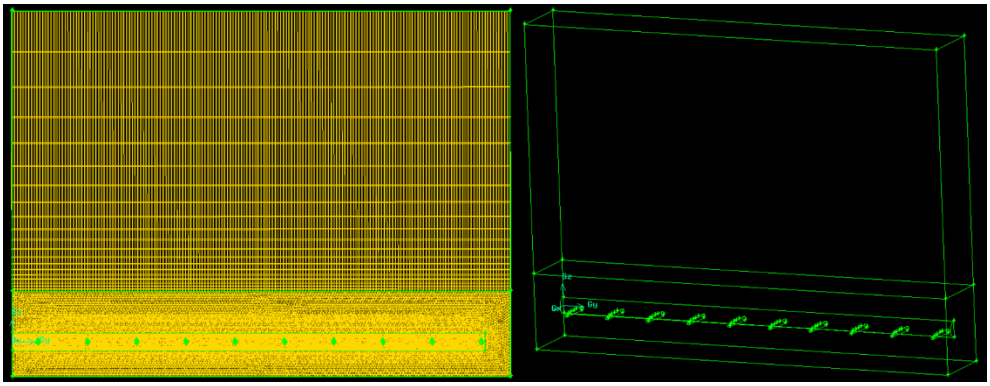

(a)

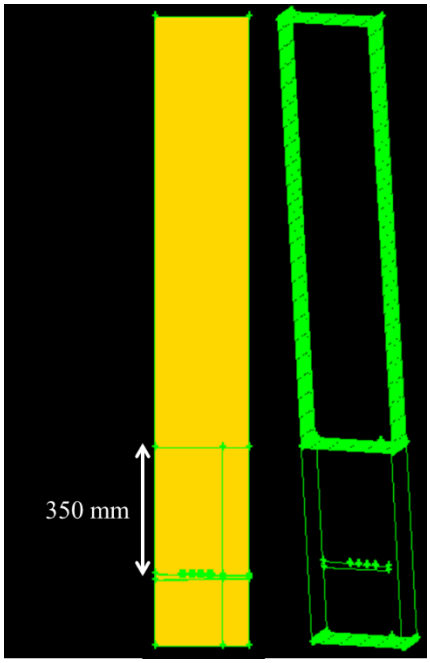

(b)

Figure 3 Mesh structure of computational domain for free bubbling regime in (a) full-scale aeration pipe and (b) full-scale FSMBR generated by GAMBIT software.

Table 1 Mesh information for various 3D aeration pipe computational geometries

Aerator with closed end (ACE) and open end (AOE) in free bubbling regime: pipe length of 1760 mm, aerator length of 180 mm, nozzles diameter of 4 mm.

Name	Origin I.D. (mm)	Varying I.D. (mm)	Number of Cells	Number of Faces	Number of Nodes
ACE-18-18	18	18	1,477,176	4,584,271	1,745,090
AOE-18-18	18	18	1,598,856	5,082,426	1,939,282
AOE-18-15	18	15	1,484,008	4,772,466	1,860,256
AOE-18-12	18	12	1,448,483	4,645,937	1,816,706
AOE-18-9	18	9	1,404,208	4,529,141	1,776,506
AOE-18-6	18	6	1,362,712	4,402,612	1,732,956
AOE-18-3	18	3	1,362,712	4,402,612	1,732,956

Aerator with AOE-18-9 in normal FSMBR system

Name	Channel Width (mm)	Pipe Length (mm)	Aerator Length (mm)	nozzles Diameter (mm)	Number of Cells	Number of Faces	Number of Nodes
PL-1520	3.5	1520	180	4	2,192,095	7,043,651	2,661,083
PL-1600	4	1600	180	4	2,192,095	7,043,651	2,661,083
PL-1760	5	1760	180	4	2,222,033	7,253,589	2,871,021
PL-2000	6.5	2000	180	4	2,256,769	7,618,325	3,235,757
PL-2240	8	2240	180	4	2,349,606	7,811,162	3,428,594

AL-130	5	1760	130	4	2,448,241	7,909,797	3,527,229
AL-150	5	1760	150	4	2,455,130	7,977,686	3,595,118
AL-180	5	1760	180	4	2,464,128	8,058,684	3,676,116
AL-210	5	1760	210	4	2,513,512	8,208,068	3,825,500
AL-230	5	1760	230	4	2,596,459	8,591,015	4,208,447
NozzleD-3	5	1760	180	3	2,590,093	8,523,649	4,141,081
NozzleD-3.5	5	1760	180	3.5	2,597,992	8,531,548	4,148,980
NozzleD-4	5	1760	180	4	2,591,504	8,525,060	4,142,492
NozzleD-5	5	1760	180	5	2,199,739	7,051,295	2,668,727
NozzleD-6	5	1760	180	6	2,257,992	7,619,548	3,236,980

Aerator with AOE-18-9 in normal FSMBR system with channel gap of 5 mm

Name	Central Pipe Diameter (mm)	Pipe Length (mm)	Aerator Length (mm)	nozzles Diameter (mm)	Number of Cells	Number of Faces	Number of Nodes
PipeD-56	56	1760	180	4	2,179,691	7,592,620	3,170,148
PipeD-48	48	1760	180	4	2,030,172	7,403,591	3,054,273

Table 2 Example mesh information for a 3D FSMBR computational geometry

FSMBR system with modified aerator of open end (MOE): Height of Membrane Plate 1200 mm, Channel width of 5 mm, Pipe length of 1760 mm, Aerator length of 180 mm, Nozzles diameter of 4 mm.

Name	Number of Cells	Number of Faces	Number of Nodes
MOE-18-9	1,404,208	4,529,141	1,776,506

2.2.2 Governing equations

3D simulations were conducted with ANSYS FLUENT 14.5. The air flow pattern and velocity distribution throughout aeration pipe and aerators was calculated by VOF (Volume of Fluid) model [27, 28]. Mass and momentum conservation equations are given as following:

$$\frac{\partial \rho}{\partial t} + \nabla(\rho \vec{u}) = 0 \tag{1}$$

$$\frac{\partial}{\partial t}(\rho \vec{u}) + \nabla(\rho \vec{u}\vec{u}) = -\nabla P + \rho \vec{g} + \rho \vec{F} + \nabla \vec{\tau} \tag{2}$$

where on the right side of Eqn. (2), the first three items represent pressure, gravitational acceleration, and external force, respectively. In each control volume, the properties of density ρ and dynamic viscosity μ were determined by volume-fraction-averaged method for an n-phase system:

$$\rho = \sum \alpha_q \rho_q \tag{3}$$

$$\mu = \sum \alpha_q \mu_q \tag{4}$$

Where,

$$\sum_{q=1}^{n} \alpha_q = 1 \tag{5}$$

Realizable k–ε model [29] was used for flow turbulence calculation, instead of standard k–ε model. This is because the Realizable model was improved to better simulate the complex secondary flow features, i.e., curvature, vortices, and rotation. Relative equations in the Realizable k–ε model for k (turbulence kinetic energy) and ε (dissipation rate) are expressed as

$$\frac{\partial}{\partial t}(\rho k) + \frac{\partial}{\partial x_j}(\rho k u_j) = \frac{\partial}{\partial x_j}\left[\left(\mu + \frac{\mu_t}{\sigma_k}\right)\frac{\partial k}{\partial x_j}\right] + G_k + G_b - \rho\varepsilon - Y_M \quad (6)$$

$$\frac{\partial}{\partial t}(\rho\varepsilon) + \frac{\partial}{\partial x_j}(\rho\varepsilon u_j) = \frac{\partial}{\partial x_j}\left[\left(\mu + \frac{\mu_t}{\sigma_\varepsilon}\right)\frac{\partial \varepsilon}{\partial x_j}\right] + \rho C_1 S\varepsilon - \rho C_2 \frac{\varepsilon^2}{k + \sqrt{\upsilon\varepsilon}} + C_{1\varepsilon}\frac{\varepsilon}{k}C_{3\varepsilon}G_b + S_\varepsilon \quad (7)$$

where

$$\mu_t = \rho C_\mu \frac{k^2}{\varepsilon}$$

$$C_1 = \max\left[0.43, \frac{\eta}{\eta + 5}\right]$$

$$\eta = S\frac{k}{\varepsilon}$$

$$S = \sqrt{2S_{ij}S_{ij}}$$

The term G_k, represents the production of turbulence kinetic energy as defined:

$$G_k = -\rho\overline{u_\iota' u_j'}\frac{\partial u_j}{\partial x_i}$$

The k–ε model accounts for the generation of k due to buoyancy by G_b and its corresponding contribution to the production of ε, which is given by

$$G_b = \beta g_i \frac{\mu_t}{Pr_t}\frac{\partial T}{\partial x_i}$$

Y_M in Equation (6) represents dilatation dissipation from turbulence due to the compressibility effect, which is normally neglected in the incompressible flows. Instead of constant, C_μ is a function of rotation rates, mean strain and the turbulence fields. C_2 and $C_{1\varepsilon}$ are constants. Turbulent Prandtl numbers of k and ε are represented by σ_k and σ_ε, respectively.

Surface tension was calculated by Continuum Surface Force (CSF) model [28]. Rather than a boundary value condition on the interface, this is modeled by pressure jump method and calculated through a source term in momentum, which is shown as:

$$p_L - p_G = \sigma\kappa \tag{8}$$

$$\vec{F}_{vol} = \sigma \frac{2\rho\kappa\nabla_{\alpha_G}}{(\rho_L + \rho_G)} \tag{9}$$

where the curvature κ is defined with divergence of the unit normal, $\hat{n}$:

$$\kappa = \nabla\hat{n}$$

$$\hat{n} = \frac{n}{|n|}, n = \nabla\alpha_q$$

2.2.3 Numerical methods and boundary conditions

The simulations were proceeded through the pressure-based solver. Momentum equations and k–ε turbulence was discretized by second order upwind scheme, and pressure-velocity coupling was solved by PISO. The volume fraction function is solved using the geometric reconstruction scheme based on piecewise linear interface calculation (PLIC). Volume flow rates for aeration were generally fixed at 1920 L/min, whilst net liquid phase velocity was set to be zero. Stationary boundary conditions were used for all of the walls with a condition of no fluid-slip at the membrane surfaces.

3. Results and Discussion

3.1 Model validation

Experimental measurements for bubble behavior have been conducted to validate the model. Bubble features were qualitatively and quantitatively compared in Table 3, Table 4 and Fig. 4. Bubble column height from the nozzles were measured for all the aerator design

cases. For the open-end aeration design, the bubble size was observed for six aerators with different side nozzle diameter between 18 to 3 mm. Experimental results showed that the bubble dimension of top apertures varied from 42 mm to 58 mm, and for the side nozzle from 65 mm to 91 mm. For the side aperture diameter larger than 9 mm, the top nozzle bubbles were around 43 mm and the side nozzle bubble were around 85 mm. Whist those increased to be around 58 mm and 80 mm as the side aperture diameter decreased to 9 mm. As the side aperture diameter decreased to be less than 9 mm, the top nozzle bubble changed little, but the side nozzle bubble size decreased to around 65 mm. The bubble frequency varied from 12 s^{-1} to 15 s^{-1} for the top and side nozzles, as the side aperture diameter decreased from 18 mm to 3 mm, which accords with the CFD results.

Moreover, the bubble size and bubble frequency of the new design were also compared with that of the traditional design. For the traditional design, which only has top apertures, the air column height was around 46 mm and the bubble frequency was 14 s^{-1} for all 4 apertures from both experiment and simulation data. The frustum aerator design with an open-end gave similar results for its top apertures but additionally the end nozzle produced large bubbles with height of averaged 78 mm and bubble frequency of 13 s^{-1}.

Table 3 Bubble dimension (mm): comparison between CFD results and experimental data for aerators of different designs with bubbling flow rate of 96 L/min

Name	Top Aperture experimental	Top Aperture simulation	Side nozzle experimental	Side nozzle simulation
ACE-18-18	45±1	47	N/A	N/A
AOE-18-18	40±2	40	91±1	88
AOE-18-15	45±1	44	84±2	86
AOE-18-12	48±2	49	80±2	82
AOE-18-9	46±2	45	80±1	77
AOE-18-6	42±1	44	72±1	70
AOE-18-3	47±2	49	65±2	66

Table 4

Bubble rising frequency: comparison between CFD results and experimental data for aerators of different designs each with air flow rate of 96 L/min

Name	Top Aperture experimental	Top Aperture simulation	Side nozzle experimental	Side nozzle simulation
ACE-18-18	15±1	13	N/A	N/A
AOE-18-18	12±1	14	12±1	14
AOE-18-15	12±1	14	12±1	14
AOE-18-12	13±1	15	13±1	15
AOE-18-9	14±1	16	13±1	16
AOE-18-6	15±1	17	12±1	17
AOE-18-3	14±1	16	13±1	16

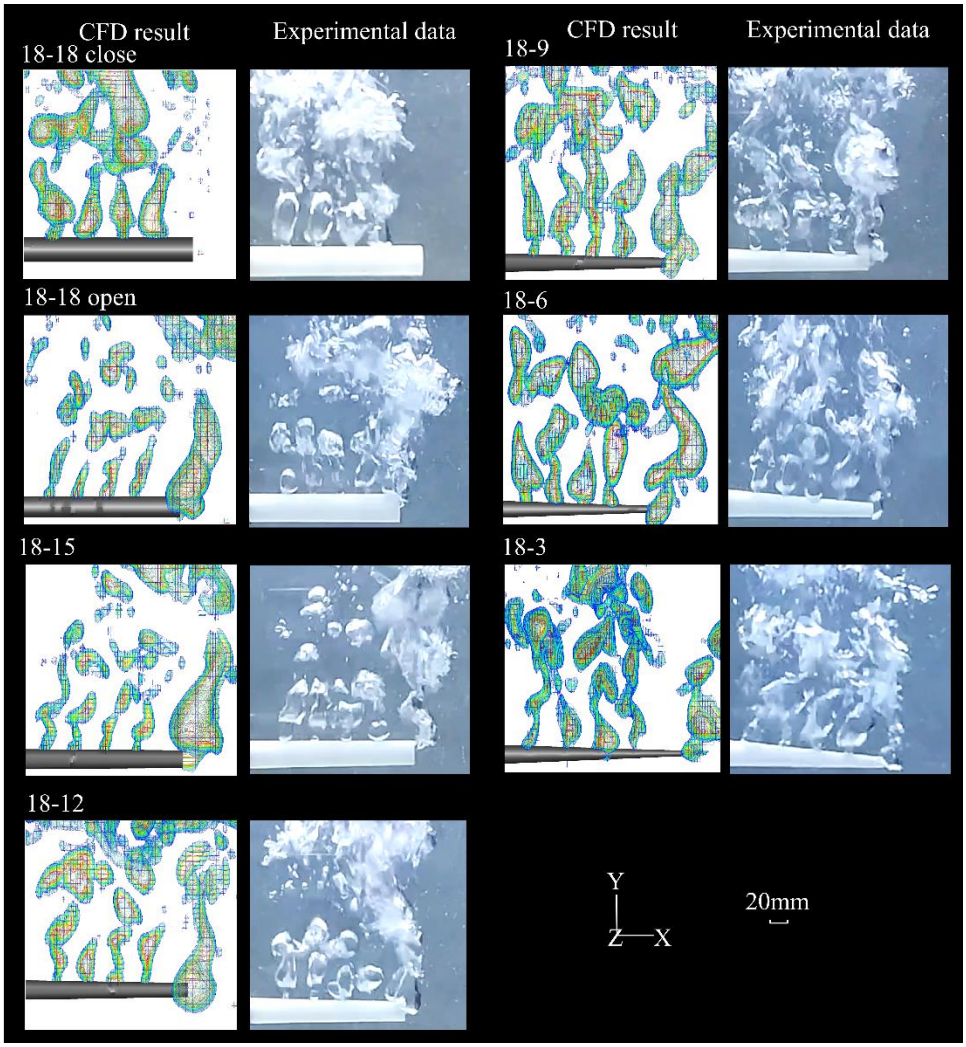

Figure 4 Comparison of CFD and experimental data for bubble features from aerators with open end diameter range from 18 to 3 mm at bubbling flow rate of 96 L/min.

The above comparison between experimental and CFD studies shows excellent agreement for the range of different aerator designs. Moreover, the difference between CFD and experiment was lower than 5%, indicating that the CFD model is a robust simulation method. Hence, the CFD model recommended itself for use in this study. The preliminary grid independence was studied, an increase in the number of cells was found to have essentially no effect on bubble shape、size and velocity. Therefore, this simulation model could be used to study the effect of changes in the design of the aerator, such as

aerator length and nozzle diameter, and changes in the length of the central supply pipe. In particular changes in velocity distribution resulting from varied pipe length, aerator length and nozzle diameter are presented. The effect upon shear stress at the membrane surface are also presented.

3.2 Design of aerator configuration

The air velocity distribution for seven designs is shown in Fig. 5 (a). The inlet air flow rate for all the cases was 1920 L/min which is the normal usage in industry for FSMBR shown in Fig. 1 which consists of 160 plates giving a total membrane area of 192 m^2. The air continuously flows through the fishbone aeration system and exits from the apertures; it is a free bubbling process. The velocity distribution and uniformity between different aerators were compared and the results are shown in Fig. 5. As the velocity contour figures (Fig. 5 (a)-(c)), show the velocity distribution in case (i) is severely nonuniform. These aerators had a closed end. However, open ends leads to improved uniformity particularly when the end aperture diameter is decreased. With end diameters between 9 and 3 mm (cases of (ii) (iii) and (iv)), the flow pattern across aerators and among different aerators was the most uniform. The details of air flow rate and its variance are plotted and quantitatively compared in Fig.5 (b) to (e).

(a) Velocity contour

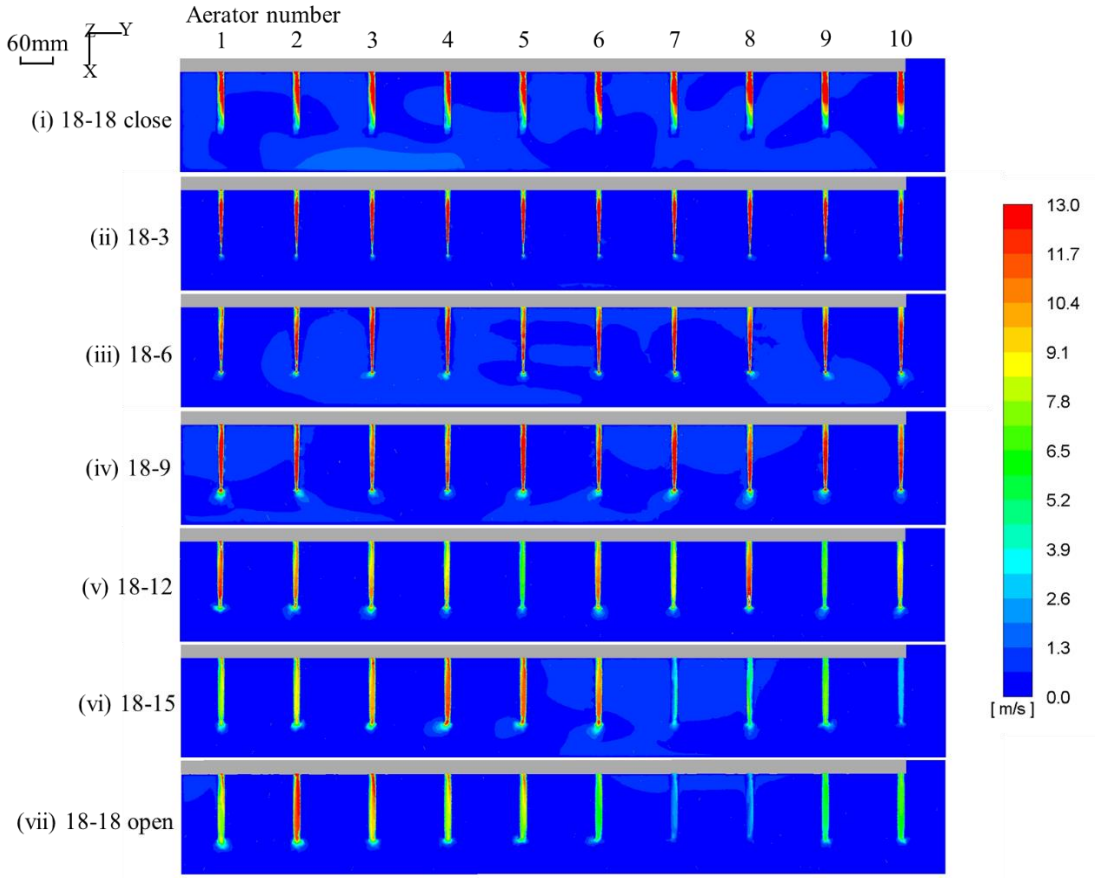

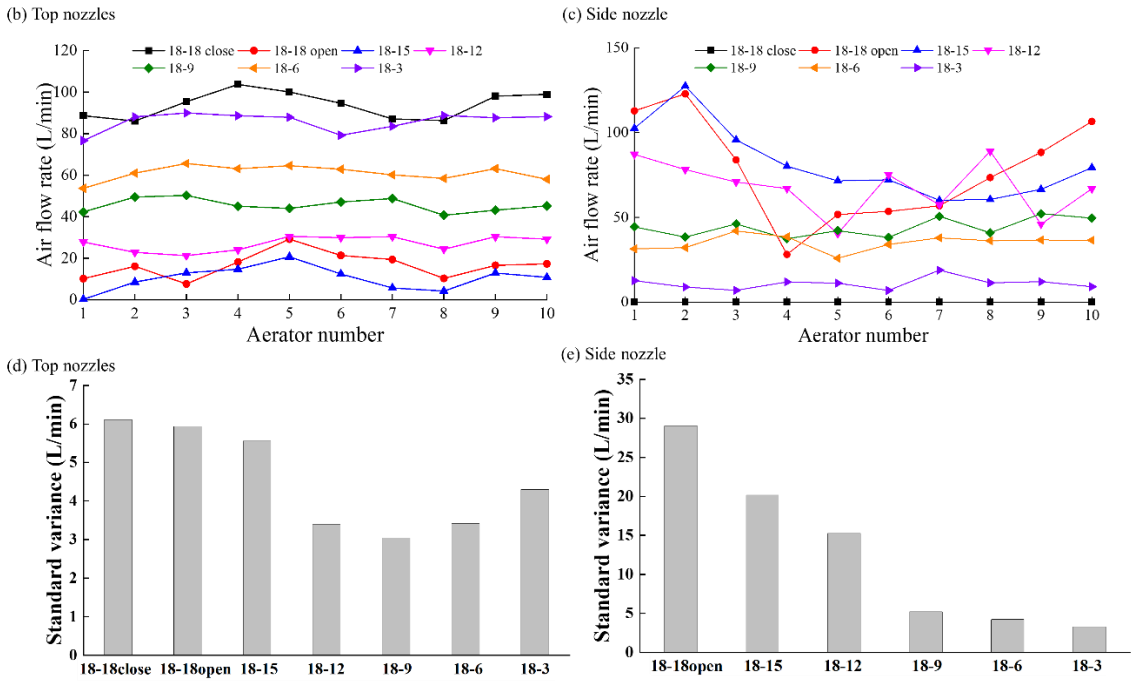

Figure 5 Comparison of the seven aerator configurations for free bubbling process with inlet aeration flow rate of 1920 L/min: (a) velocity distribution through the whole pipe and aerators; (b) sum of flow rate for four top nozzles; (c) flow rate of side nozzle; (d) standard variance for the sum flow rate of four top nozzles; (e) standard variance for side nozzle flow rate.

Quantitative evaluation of the uniformity of the air velocity is provided through the evaluation of the standard variance of flow rate of the ten aerators. As shown in Fig. 5 (d) and (e), the first three cases (18-18 closed, 18-18 open, and 18-15) had high variance of over 5.5 and 20 L/min for top and end nozzles, respectively. As the end opening diameter decreased to 12 mm, the variance decreased to be 3.4 and 15 L/min, respectively. With an end diameter of less than 9 mm the velocity variance decreased to be 3 to 4.9 L/min for top and end nozzles. Overall the 18-9 design gives excellent uniformity.

According to previous experience evaluating an open-ended aerator [26], the requirements for inducing sufficiently strong hydrodynamic effects so as to exceed the

necessary shear stress on each membrane wall were (a) total air flow rate from the top four nozzles of >40 L/min, and (b) flow from the end nozzle >18 L/min. From Fig. 5, the structures with open-end diameter of 9 and 6 mm met both requirements. Also the end opening has the function of allowing any sediment inside an aerator to be discharged and thus the larger nozzle is to be preferred. Therefore, the 18-9 structure was chosen as the basis for further study and optimization as detailed in the following sections.

3.3 Variation in length of Central Pipe

The channel gap between every pair of membrane plate was changed from 3.5 to 8 mm and the consequential change in the length of the central pipe was from 1520 to 2240 mm (160 membrane plates with thickness of 6 mm). The velocity distribution and flow rate for different pipe lengths are compared in Fig. 6. In the case of 2240 mm length, the flow rate of top nozzles was below 40 L/min for the first 6 aerators and then over 40 L/min for the rest as shown in Fig. 6 (b). The variance for the top nozzles (Fig. 6 (d)) was around 3 L/min for different pipe lengths from 1520 to 2240 mm, with somewhat lower variance for the longer lengths. The major difference between the five designs was observed in the end nozzle variance. For pipe lengths below 1760 mm, as shown in Fig. 6 (e), the variance was over 15 L/min but less than 10 L/min for the three cases of 1760 to 2240 mm. Thus for a more stable, more uniform velocity distribution among the ten aerators, a channel gap of 5 to 8 mm (which corresponds to a central pipe length of 1760 to 2240 mm) is, in general, to be preferred.

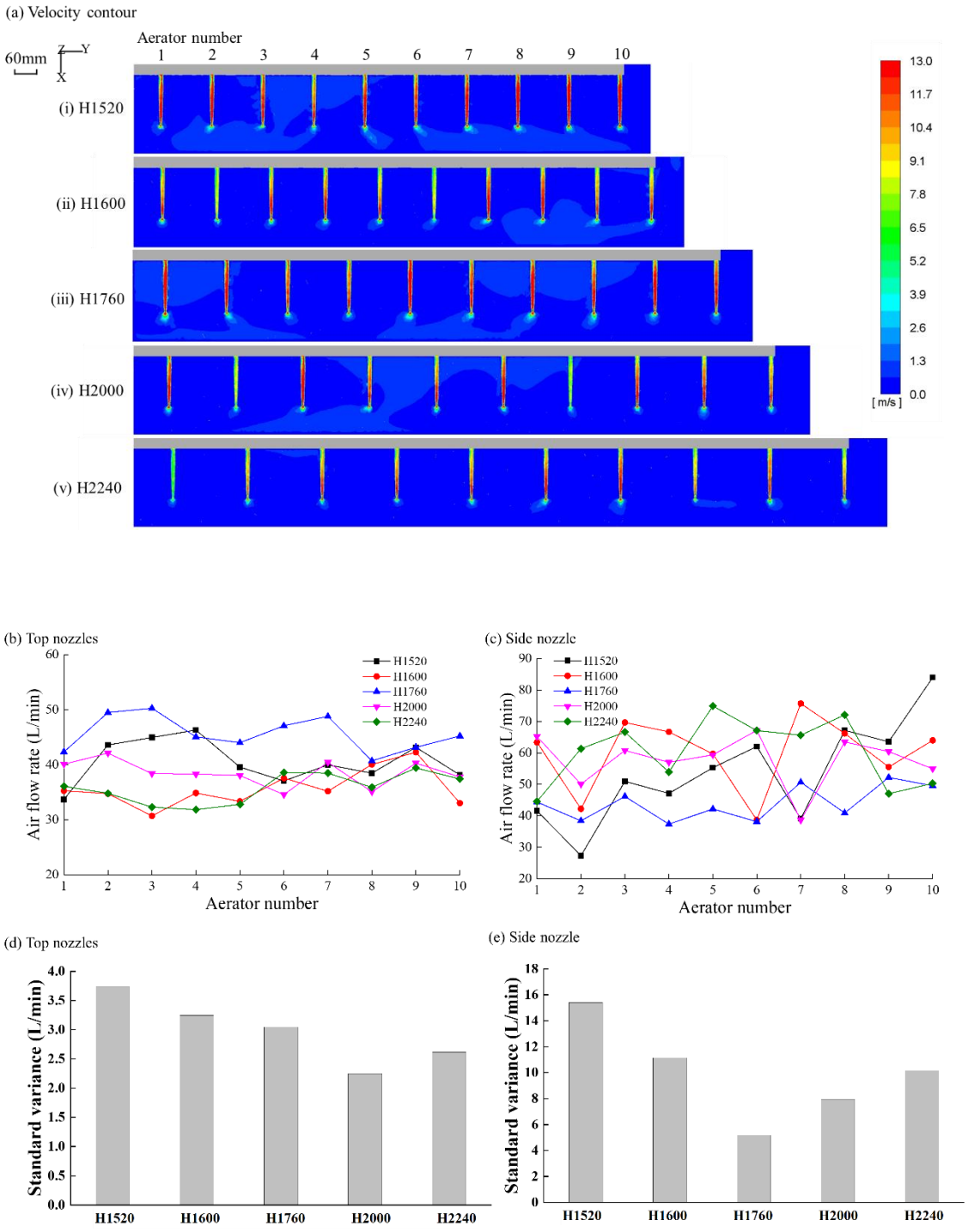

Figure 6 Comparison of various aeration pipe length with inlet flow rate of 1920 L/min: (a) velocity distribution through the whole pipe and aerators; (b) sum of flow rate for four top nozzles; (c) flow rate of side nozzle; (d) standard variance for the sum flow rate of four top nozzles; (e) standard variance for side nozzle flow rate.

3.4 Variation of aerator length

Based on the frustum 18-9 structure, the aerator length was varied from 130 to 230 mm in order to determine the optimal length of aerator whilst keeping the following fixed: aerator was frustum 18-9, the channel gap was 5 mm, and central pipe length was 1760 mm. Fig. 7 gives the velocity and flowrate distributions. Fig. 7 indicates that the aerator length of 130 to 210 mm could provide an uniform air velocity distribution. Since the case of length 180 mm had smallest variance and satisfied the flowrate requirements for top and side nozzles as mentioned in section 3.2, an aerator length of 180 mm was the optimal.

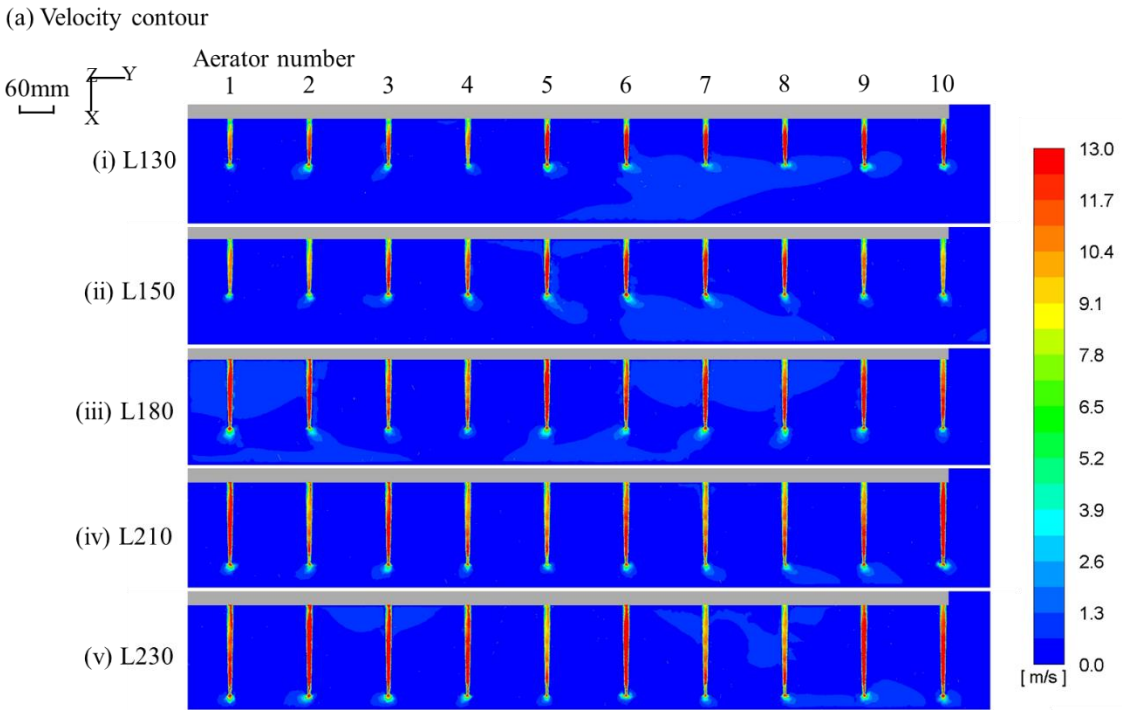

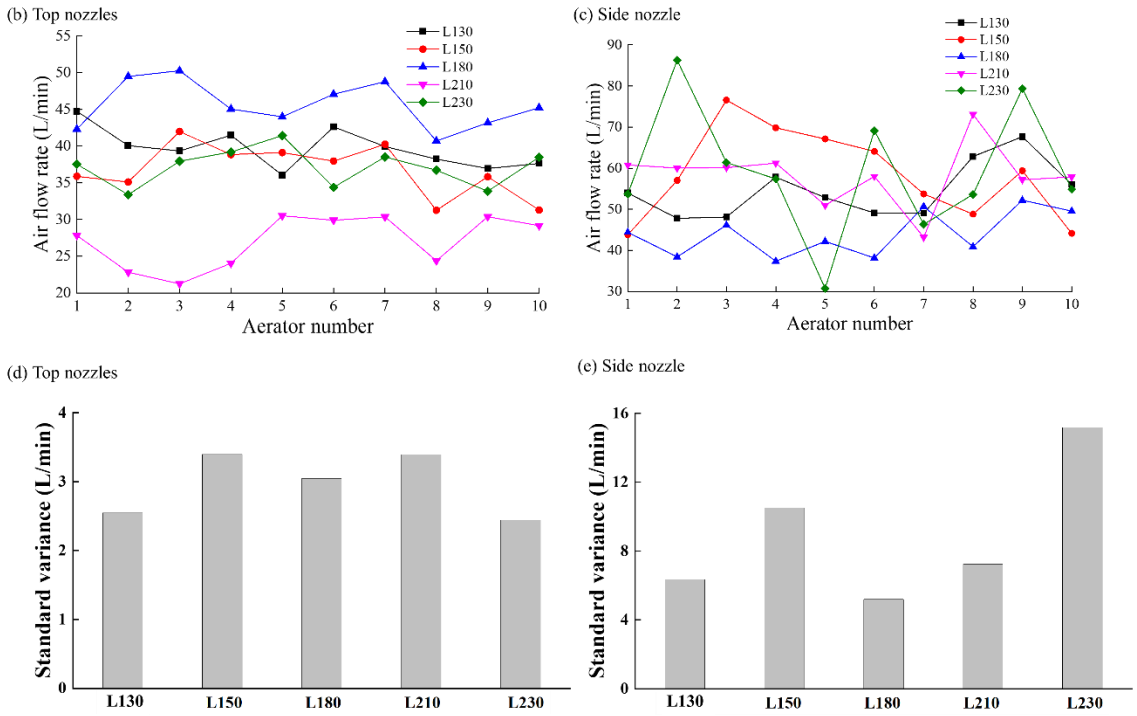

Figure 7 Comparison of various aerator length with inlet flow rate of 1920 L/min: (a) velocity distribution through the whole pipe and aerators; (b) sum of flow rate for four top nozzles; (c) flow rate of side nozzle; (d) standard variance for the sum flow rate of four top nozzles; (e) standard variance for side nozzle flow rate.

3.5 Variation of nozzle diameter

The top nozzle diameter on each aerator was varied from 3 to 6 mm whilst keeping the following fixed: the channel gap was 5 mm, aerator was frustum 18-9 with length of 180 mm, and central pipe length was 1760 mm. In Fig. 8, it showed that the flow rate from the top nozzles increased as the nozzle diameter increased with all top nozzle flow rates being above 40 L/min for nozzles larger than 3.5 mm diameter. With increasing flow through the top nozzles there was correspondingly less flow through the end nozzle but in all cases the end nozzle flow rate was >18 L/min. The trends in the variances of flow rate from the top nozzles was opposite to that from the end nozzles; for diameters 5 and 6 mm, the standard variance of top nozzles was the highest at 7 L/min but the corresponding end nozzle flow rate variance was lowest at 3.5 L/min. Considering both top and end nozzle, a diameter of 4 mm will be the most appropriate.

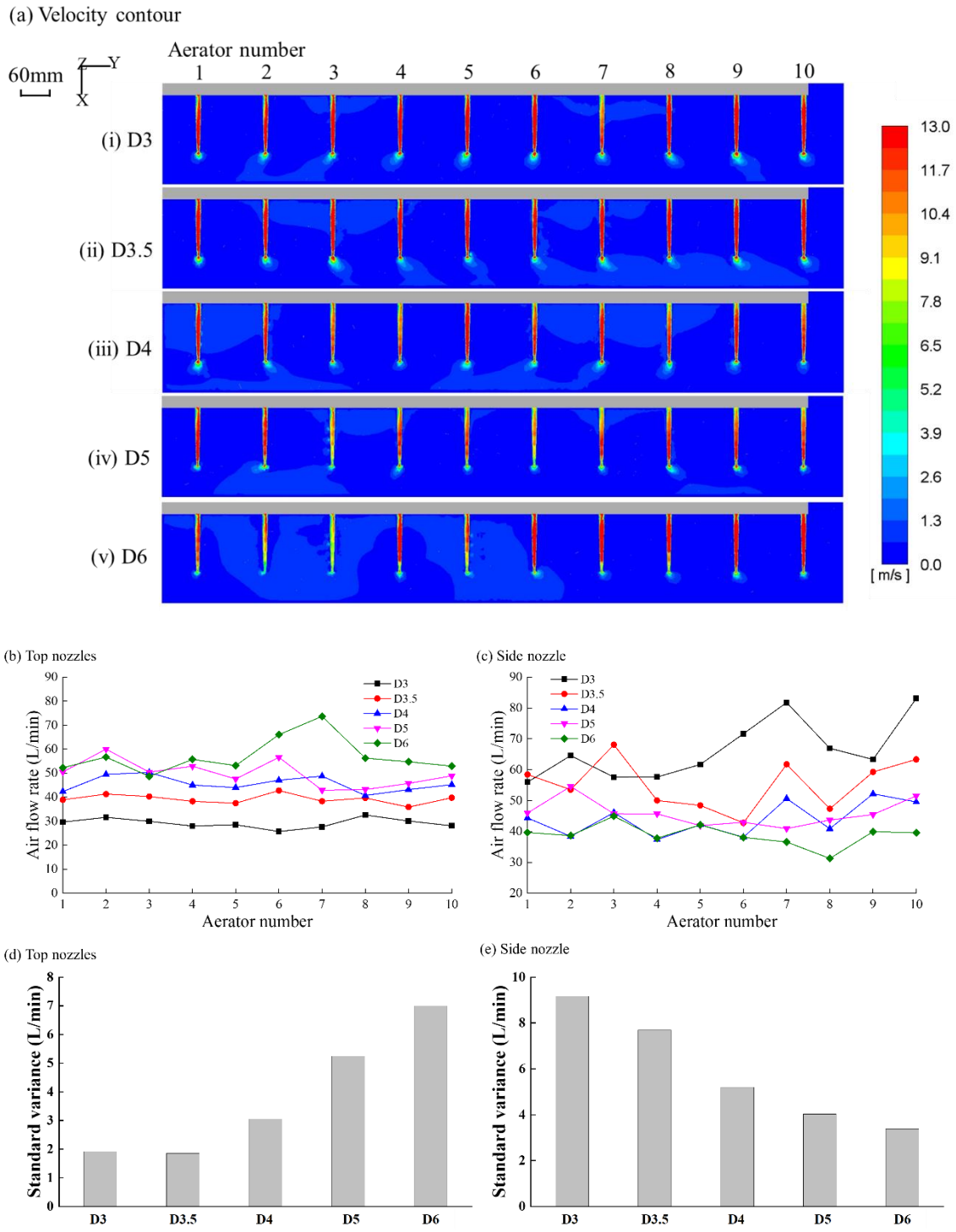

Figure 8 Comparison of various nozzles diameter with inlet flow rate of 1920 L/min, the channel gap was 5 mm, aerator was frustum 18-9 which length was 180 mm, and central pipe length was 1760 mm: (a) velocity distribution through the whole pipe and aerators; (b) sum of flow rate for four top nozzles; (c) flow rate of side nozzle; (d) standard variance for the sum flow rate of four top nozzles; (e) standard variance for side nozzle flow rate.

3.6 Modification of Central Pipe diameter

Maintaining an optimal structure of frustum 18-9 aerator design as invariant, the influence of the central pipe diameter was investigated. Specifically it was decreased from standard 64 mm to 56 and 48 mm. As illustrated in Fig. 9, the flow rates from the top nozzles were similar for the two cases of pipe diameter 56 and 48 mm (the average values being 47 and 46 L/min respectively). The average value for the standard case is 44 L/min. Increasing the resistance to flow down the central tube increases the flow through the end nozzles. The average values for the pipes of 64 mm to 56 and 48 mm were 43, 48, 49 L/min respectively. The variance of top nozzle flow rates decreased around 40% at pipe diameter of 56 and 48 mm, compared to the standard 64 mm; whilst that of end nozzle was similar around 5 L/min. Considering both the flow rate values and smaller variance, pipe diameter of 56 mm was determined to be the most appropriate size.

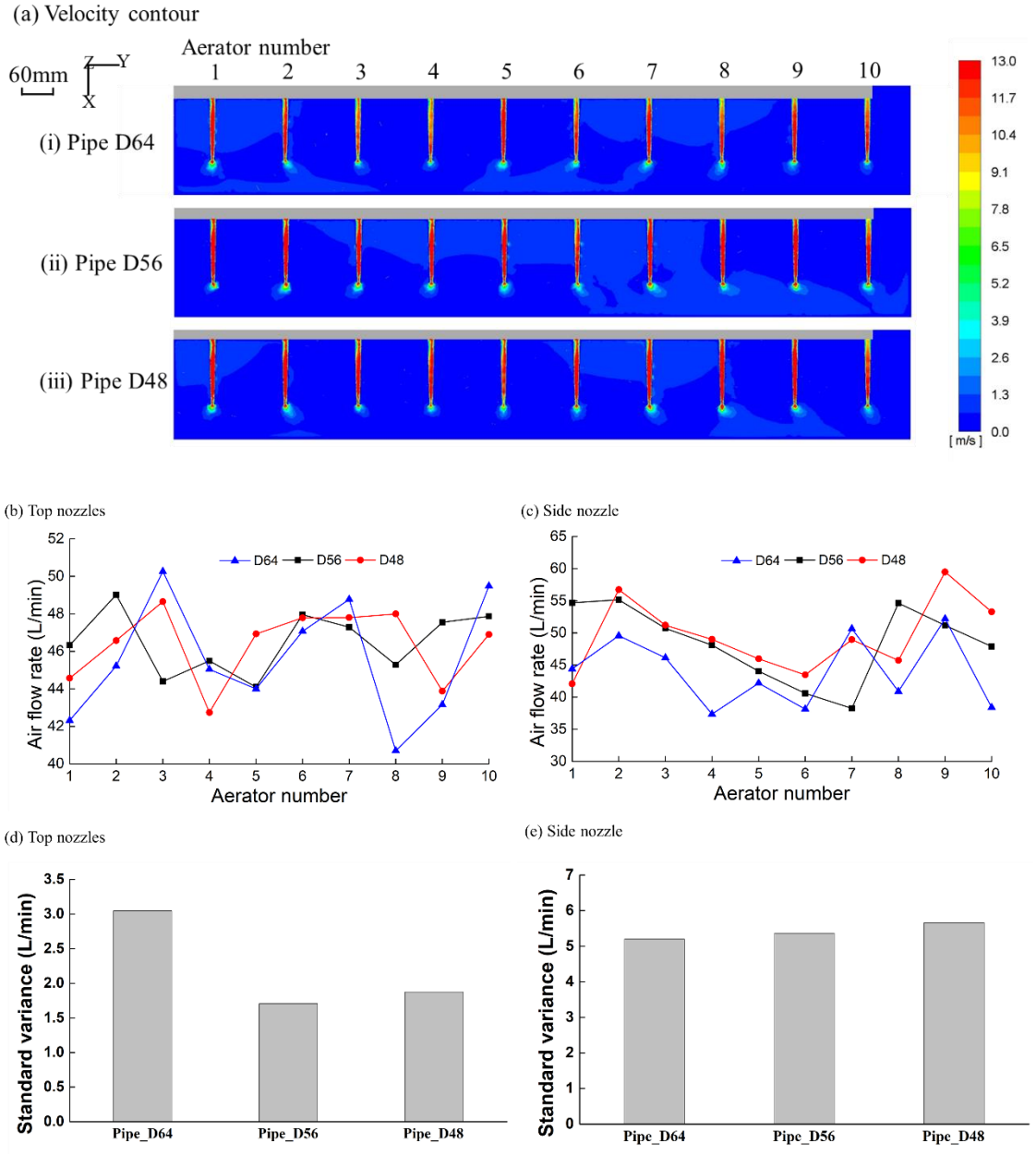

Figure 9 Comparison of various central pipe diameter with inlet flow rate of 1920 L/min, the channel gap was 5 mm, aerator was frustum 18-9 which length was 180 mm, and central pipe length was 1760 mm, nozzle diameter was 4 mm: (a) velocity distribution through the whole pipe and aerators; (b) sum of flow rate for four top nozzles; (c) flow rate of side nozzle; (d) standard variance for the sum flow rate of four top nozzles; (e) standard variance for side nozzle flow rate.

3.7 Shear stress comparison

The optimal structure determined above features the new frustum 18-9 aerator design with a top nozzle diameter of 4mm and an aerator length of 180 mm attached to a central pipe of diameter 56 mm and length 1760 mm. For this design, the shear stress on the membrane walls induced from free bubbling was predicted and compared with the values generated using a conventional fishbone aerator. The former is labelled 'Modified PipeD56 18-9' and the latter 'Conventional PipeD64 18-18 closed'. A comparison is also made with 'Modified PipeD64 18-9' in order to check whether a central pipe diameter of 56mm is superior to one of 64 mm or not. In all cases the air supply was 1920 L/min and the channel gap was 5 mm.

In the overall FSMBR unit there are 10 pairs of aerators and between each aerator there are 16 channels. The middle unit in the FSMBR was examined in detail. Due to the symmetry it is sufficient to examine a section comprising 8 channels in which there is further symmetry between the two membrane walls on each side. Hence hydrodynamics results on 8 membrane walls were calculated.

In Fig. 10 (a) and (b), the bubble distribution and shear stress are compared. In Fig. 10 (c), the x-axis indicates the location of the membrane surface with respect to the aerator – '1' is at the closest position to an aerator whilst '8' is midway between two aerators; the y-axis gives the corresponding average shear stress. It can be seen that larger bubbles are more numerous in both modified cases than the conventional case, especially in channels 2 – 6. This resulted in a shear stress enhancement as shown in Fig. 10 (b) and (c). The shear stress was over 1.5 Pa for all the walls in the PipeD 56 18-9 case. By contrast only 75% of

the membrane walls could reach more than 1.2 Pa in the 18-9 case and this level was reached by just 25% in the conventional 18-18 closed-end system.

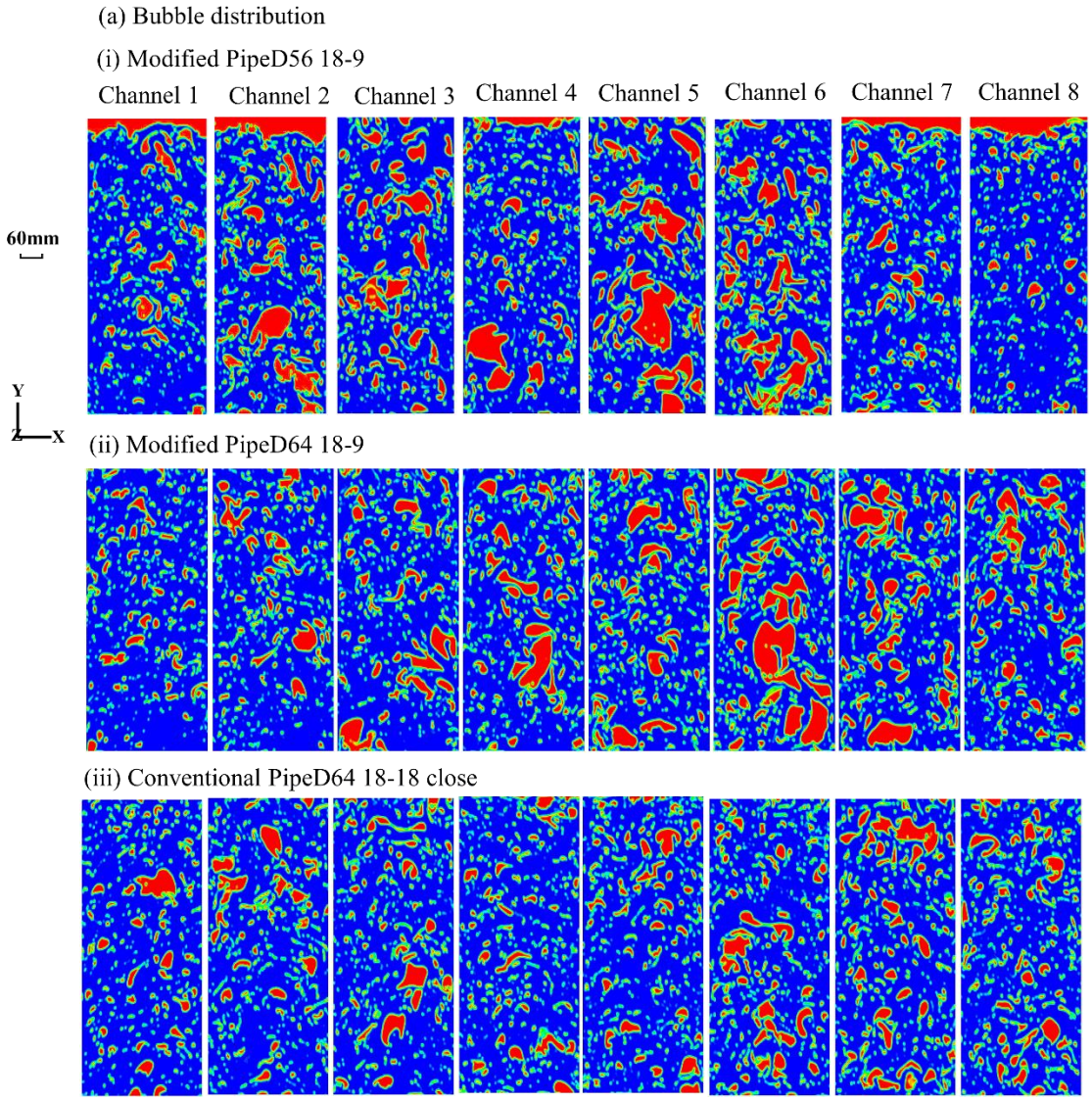

(b) Shear stress

(i) Modified PipeD56 18-9

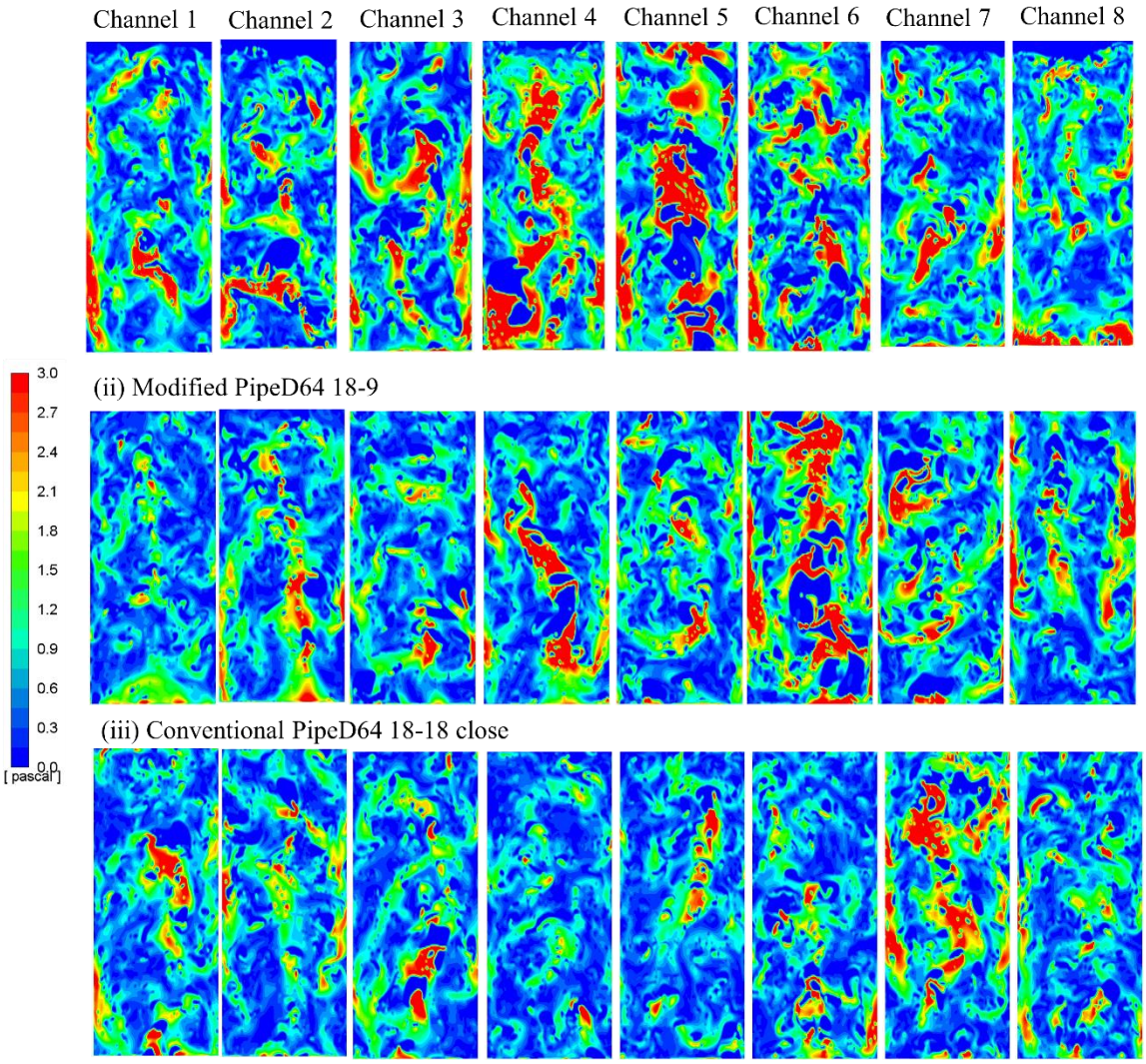

(c) Average shear stress

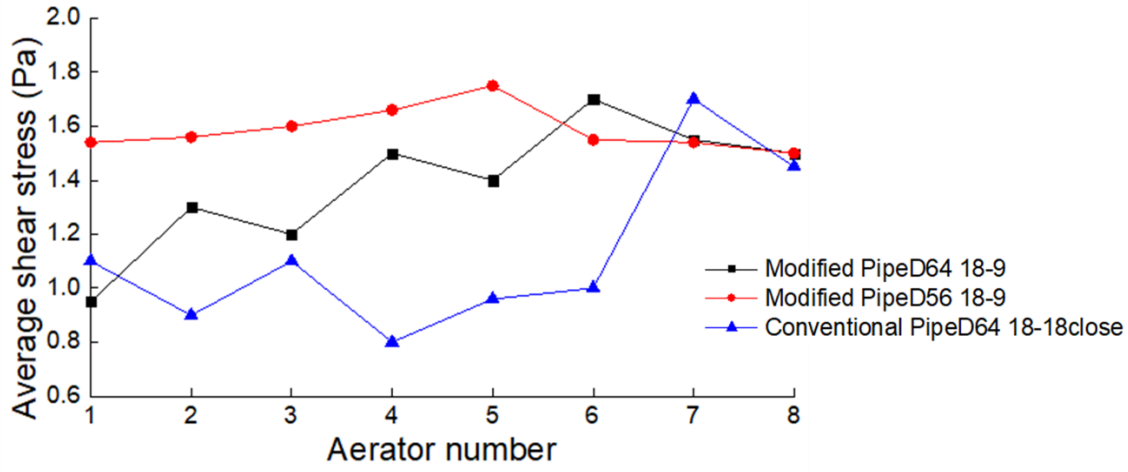

Figure 10 Comparison of hydrodynamic effect between designs of frustum 18-9 open-end structure and traditional 18-18 closed-end; (a) bubble distribution; (b) shear stress; (c) average shear stress. The "Membrane position" indicates the position of a membrane wall with respect to the aerator – '1' is at the closest position to an aerator whilst '8' is midway between two aerators

Our research to this point has shown that for a given air input the hydrodynamic effect can be enhanced through the use of frustum open-ended aerators of the 18-9 design optimization above. Based on this, the central pipe diameter could be changed to enhance the shear stress on membrane walls, which was significant for the fouling control. As shown in Table 5, the number of effective channel coverage from one aerator was compared, it was 4 channels in conventional case, whilst the number increased to be 8 and 16 in modified case of 18-9 structure, with pipe diameter of 64 and 56 mm respectively. Therefore, through the optimization of aerator structure and pipe designs, the effective channel coverage was enhanced by 25 and 75%, compared to the conventional aeration.

Table 5 Comparison of hydrodynamic effect from different pipe designs in free bubbling MBRs

FSMBR with channel gap 5 mm, including 160 sheets of membranes sized 510×6×1200 mm (L×T×H)

Name	Number of effective channel coverage of one aerator	Percentage of effective channels increased (%)
Modified PipeD56 18-9	16	75*
Modified PipeD64 18-9	8	25*
Conventional PipeD64 18-18 close	4	N/A

*data was calculated by difference of modified and conventional effective channel number over the total channel number of 16 by one aerator, i.e., $(N_{D56\_18\text{-}9}\text{-}N_{D64\_18\text{-}18})/N_{total}$ and $(N_{D64\_18\text{-}9}\text{-}N_{D64\_18\text{-}18})/N_{total}$.

4. Concluding Remarks

Several aerator designs were proposed and compared for free bubbling process *in silico* for large module (160 membrane sheets) of full-scale FSMBR. Simulations indicate that a frustum aerator of diameter-varying of 18 to 9 mm with an open-end aperture can be optimized to achieve beneficial hydrodynamics. It was found that the optimal design featured pipe length 1760 mm, aerators length 180 mm, and top nozzles diameter 4 mm could provide uniform velocity distribution among all aerators. Based on this aerator design, central pipe diameter was decreased to be 56 mm to further enhance the hydrodynamic effect. The bubbly flow from a single branch aerator can cover 16 channels. Bubble behavior and shear stress development for different conditions of aeration velocity was calculated. Comparing with the conventional 18-18 closed design, the effective channel coverage was enhanced through the frustum 18-9 design.

Acknowledgements

This work was supported by grants from the National Key R&D Program of China (2018YFC1903205), Ministry of Science and Technology; the Bureau of Frontier Sciences and Education (QYZDB-SSW-DQC044); the Bureau of International Cooperation (132C35KYSB20160018); the Chinese Academy of Sciences and the Joint Project between CAS-CSIRO (132C35KYSB20170051); FJIRSM&IUE Joint Research Fund (No. RHZX-2019-002); National Natural Science Foundation of China (No. 52100047) and the Fundamental Research Funds for the Central Universities, Nankai University (0085). The authors would like to thank the grant of “antifouling membranes and slug bubbling flat sheet membrane bioreactors for the next generation wastewater treatment” and Oxiamembrane Co.Ltd for technical support. RWF acknowledges the support provided by an APEX project on water reuse that has been supported by the Royal Society in partnership with the British Academy and the Royal Academy of Engineering together with

generous support from the Leverhulme Trust. The authors also thank Mr. Xingbiao Chen and Dr. Olusegun Abass for their help and industrial perspective.

References

[1] R. Kumari, H. Ankit, S. Basu, Reclamation of water from dairy wastewater using membrane bioreactor (MBR) – Membrane filtration processes, Materials Today: Proceedings, (2021).

[2] M.L. Christensen, M.K. Jørgensen, G. Van De Staey, L. De Cock, I. Smets, Hydraulic resistance and osmotic pressure effects in fouling layers during MBR operations, Journal of Membrane Science, 627 (2021) 119213.

[3] G. Hu, X. Liu, Z. Wang, X. Du, X. Wang, Comparison of fouling behaviors between activated sludge suspension in MBR and EPS model solutions: A new combined model, Journal of Membrane Science, 621 (2021) 119020.

[4] S. Tabraiz, B. Shamurad, E. Petropoulos, M. Quintela-Baluja, A. Charlton, J. Dolfing, P.J. Sallis, Mitigation of membrane biofouling in membrane bioreactor treating sewage by novel quorum quenching strain of Acinetobacter originating from a full-scale membrane bioreactor, Bioresource Technology, 334 (2021) 125242.

[5] M. Yang, M. Liu, D. Yu, J. Zheng, Z. Wu, S. Zhao, J. Chang, Y. Wei, Numerical simulation of scaling-up for AEC-MBRs regarding membrane module configurations and cyclic aeration modes, Bioresource Technology, 245 (2017) 933-943.

[6] E. Suard, R. Clément, Y. Fayolle, M. Alliet, C. Albasi, S. Gillot, Electrical resistivity tomography used to characterize bubble distribution in complex aerated reactors: Development of the method and application to a semi-industrial MBR in operation, Chemical Engineering Journal, 355 (2019) 498-509.

[7] M. Mayer, R. Braun, W. Fuchs, Comparison of various aeration devices for air sparging in crossflow membrane filtration, Journal of Membrane Science, 277 (2006) 258-269.

[8] M. Liu, M. Yang, M. Chen, D. Yu, J. Zheng, J. Chang, X. Wang, C. Ji, Y. Wei, Numerical optimization of membrane module design and operation for a full-scale submerged MBR by computational fluid dynamics, Bioresource Technology, 269 (2018) 300-308.

[9] E. Radaei, X. Liu, K.H. Tng, G. Merendino, F.J. Trujillo, P.R. Bérubé, G. Leslie, Numerical and experimental investigation of pulse bubble aeration with high packing density hollow-fibre MBRs, Water Research, 160 (2019) 60-69.
[10] K. Zhang, Z. Cui, R.W. Field, Effect of bubble size and frequency on mass transfer in flat sheet MBR, Journal of Membrane Science, 332 (2009) 30-37.
[11] E. Radaei, X. Liu, K.H. Tng, Y. Wang, F.J. Trujillo, G. Leslie, Insights on pulsed bubble control of membrane fouling: Effect of bubble size and frequency, Journal of Membrane Science, 554 (2018) 59-70.
[12] X. Liu, Y. Wang, T.D. Waite, G. Leslie, Numerical simulation of bubble induced shear in membrane bioreactors: Effects of mixed liquor rheology and membrane configuration, Water Research, 75 (2015) 131-145.
[13] R. Field, K. Zhang, Z. Cui, B.-K. Hwang, Flat sheet MBRs: Analysis of TMP rise and surface mass transfer coefficient, Desalination and Water Treatment - DESALIN WATER TREAT, 35 (2011) 82-91.
[14] Z.F. Cui, Experimental investigation on enhancement of crossflow ultrafiltration with air sparging, Effective Membrane Processes—New Perspectives., Mechanical Engineering Publications Ltd, London, (1993) 237–245.
[15] M. Yang, D. Yu, M. Liu, L. Zheng, X. Zheng, Y. Wei, F. Wang, Y. Fan, Optimization of MBR hydrodynamics for cake layer fouling control through CFD simulation and RSM design, Bioresource Technology, 227 (2017) 102-111.
[16] A. Pinilla, J.C. Berrio, E. Guerrero, J.P. Valdés, D. Becerra, P. Pico, L. Vargas, S. Madsen, T.R. Bentzen, N. Ratkovich, CFD modelling of the hydrodynamics in a filtration unit with rotating membranes, Journal of Water Process Engineering, 36 (2020) 101368.
[17] X. Liu, Y. Wang, Y. Shi, Q. Li, P. Dai, J. Guan, T.D. Waite, G. Leslie, CFD modelling of uneven flows behaviour in flat-sheet membrane bioreactors: From bubble generation to shear stress distribution, Journal of Membrane Science, 570-571 (2019) 146-155.
[18] P. Wei, K. Zhang, W. Gao, L. Kong, R. Field, CFD modeling of hydrodynamic characteristics of slug bubble flow in a flat sheet membrane bioreactor, Journal of Membrane Science, 445 (2013) 15-24.
[19] K. Zhang, Z. Cui, R. Field, Effect of bubble size and frequency on mass transfer in flat sheet MBR, Journal of Membrane Science, 332 (2009) 30-37.

[20] K. Zhang, R.W. Field, Z. Cui, Measurement of the mass transfer coefficients in submerged flat sheet membrane systems., in: The conference of the European Membrane Society., 2006.
[21] K. Zhang, P. Wei, M. Yao, R.W. Field, Z. Cui, Effect of the bubbling regimes on the performance and energy cost of flat sheet MBRs, Desalination, 283 (2011) 221-226.
[22] B. Wang, K. Zhang, R.W. Field, Optimization of aeration variables in a commercial large-scale flat-sheet MBR operated with slug bubbling, Journal of Membrane Science, 567 (2018) 181-190.
[23] B. Wang, K. Zhang, R.W. Field, Slug bubbling in flat sheet MBRs: Hydrodynamic optimization of membrane design variables through computational and experimental studies, Journal of Membrane Science, 548 (2018) 165-175.
[24] B. Wang, K. Zhang, R. Field, Novel Aeration of a Large-Scale Flat Sheet MBR: a CFD and Experimental Investigation, AIChE Journal, 64 (2018).
[25] B. Wang, K. Zhang, R.W. Field, Novel economical three-stage slug bubbling process in a large-scale flat-sheet membrane bioreactor of double deck configuration, AIChE Journal, 66 (2020).
[26] B. Wang, Y. Zhang, G. Zhang, K. Zhang, R.W. Field, Innovation and optimization of aeration in free bubbling flat sheet MBRs, Journal of Membrane Science, 635 (2021) 119522.

[27] C.W. Hirt, B.D. Nichols, Volume of fluid (VOF) method for the dynamics of free boundaries, Journal of Computational Physics, 39 (1981) 201-225.

[28] J.U. Brackbill, D.B. Kothe, C. Zemach, A continuum method for modeling surface tension, Journal of Computational Physics, 100 (1992) 335-354.

[29] T.-H. Shih, W.W. Liou, A. Shabbir, Z. Yang, J. Zhu, A new k-ϵ eddy viscosity model for high Reynolds number turbulent flows, Computers & Fluids, 24 (1995) 227-238.

[30] http://www.oxiamem.com